Supporting Information

Influence of Deposition Pressure on the Film Morphologies, Structures and Mobilities for Different-Shaped Organic Semiconductors

Yi Li,[a] Shuang Chen,[b] Qi Liu,[a] Yun Li,[c] Yi Shi,[c] Xizhang Wang,[a,*] Jing Ma,[a,*] and Zheng Hu[a]

[a] Key Laboratory of Mesoscopic Chemistry of MOE, Jiangsu Provincial Lab for Nanotechnology, School of Chemistry and Chemical Engineering, Nanjing University, Nanjing 210093, China

[b] Department of Chemistry and Nebraska Center for Materials and Nanoscience, University of Nebraska-Lincoln, Lincoln, Nebraska 68588, United States

[c] School of Electronic Science and Engineering, Nanjing University, Nanjing 210093, China

E-mail: wangxzh@nju.edu.cn; majing@nju.edu.cn Tel: (+86) 25-83593696

Index

SI 1. The evaporation temperatures (T_e) of organic semiconductors under different P_{dep}.

Table S1

Samples	P_{dep} (Pa)	T_e (℃)
$F_{16}CuPc$	10^{-4}	320-350
	10^{-3}	320-350
	10^{-2}	330-360
	10^{-1}	370-400
pentacene	10^{-4}	130-170
	10^{-3}	130-170
	10^{-2}	140-180
	10^{-1}	170-210
	2	220-260
	10	240-300
TIPS-pentacene	10^{-4}	140-180
	10^{-3}	140-180
	10^{-2}	160-200
	10^{-1}	190-230
C_{60}	10^{-4}	310-370
	10^{-3}	310-370
	10^{-2}	320-390
	10^{-1}	340-410

SI 2. Starting configurations for molecular dynamic simulations.

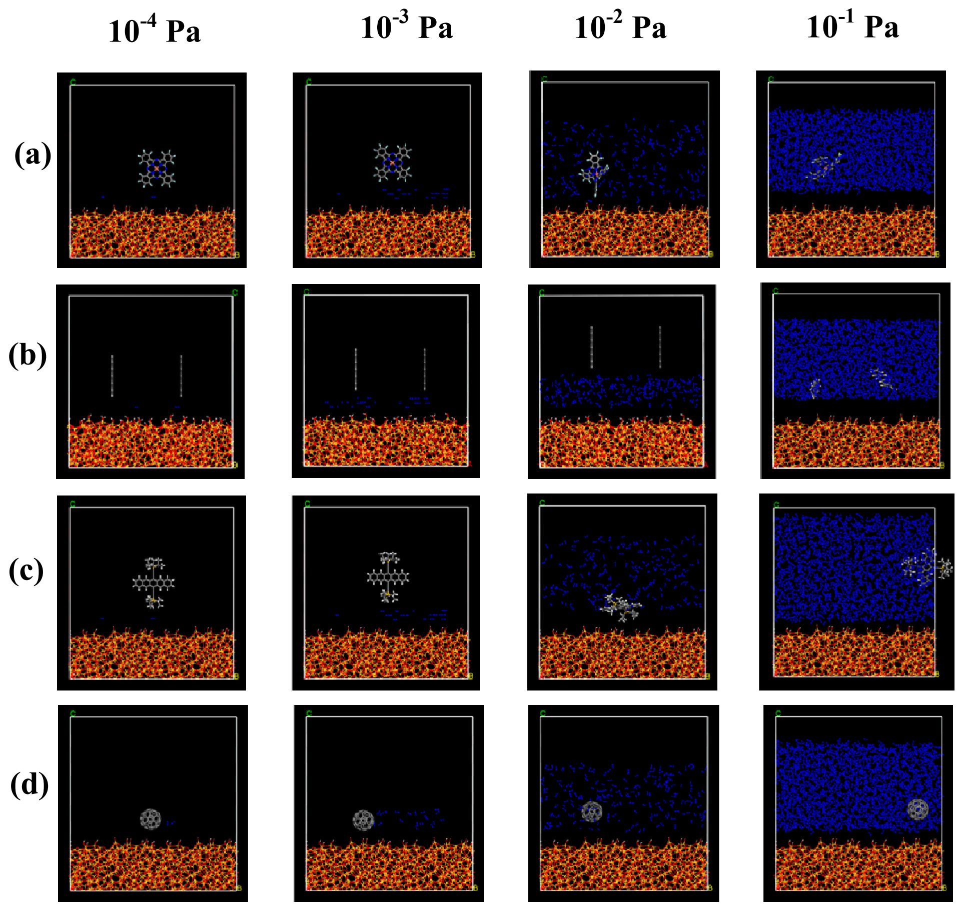

Figure S1. Starting configurations of molecular dynamic simulations for $F_{16}CuPc$ (a), pentacene (b), TIPS-pentacene (c), and C_{60} (d) molecules deposited under different P_{dep}. The number of deposited molecules ($F_{16}CuPc$, pentacene, TIPS-pentacene, and C_{60}) versus N_2 molecules was estimated by the collision theory according to the experimental condition.

SI 3. AFM images of sub-monolayer organic films.

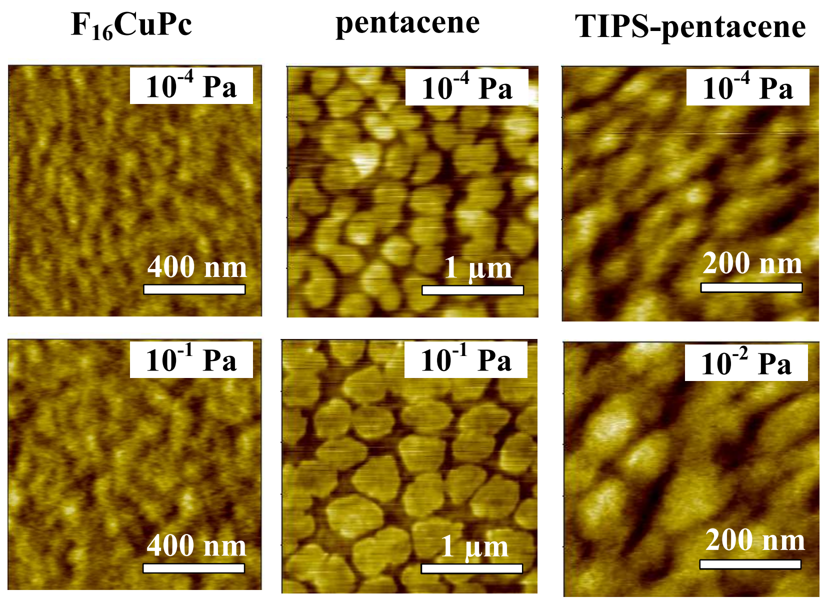

Figure S2. AFM images of sub-monolayer $F_{16}CuPc$, pentacene and TIPS- pentacene films deposited under10^{-4} and 10^{-1} (or 10^{-2}) Pa.

Note: The increased grain sizes of sub-monolayer films are obtained under high P_{dep} of 10^{-1} or 10^{-2} Pa, suggesting the decreased nucleation density, which probably due to the enhanced collision and diffusion of organic semiconductor molecules under high P_{dep}.[S1, S2]

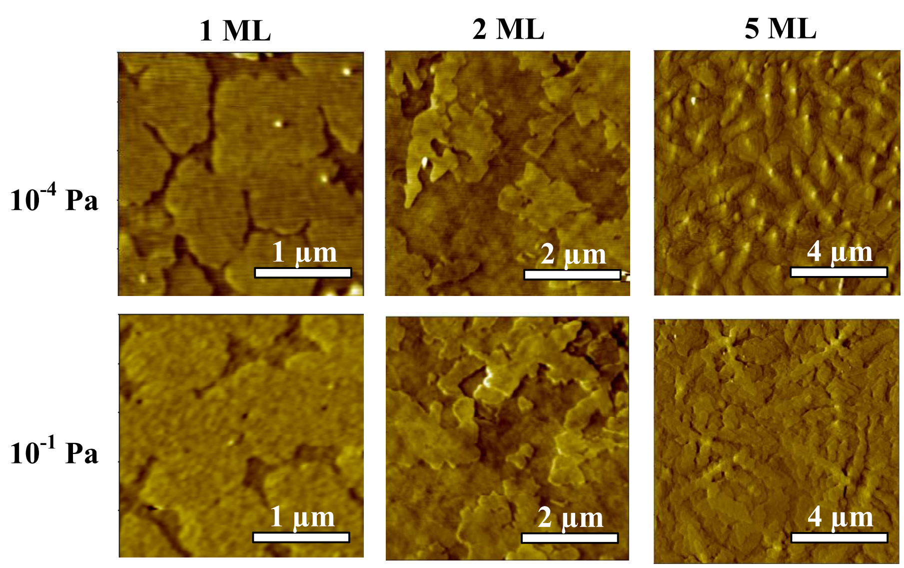

Figure S3. AFM images for pentacene films with the thickness of 1, 2 and 5 molecular layers (ML) deposited under10^{-4} and 10^{-1} Pa.

Note: The Stranski–Krastanov growth mode (layer-plus-island mode) is observed for the films deposited under both 10^{-4} and 10^{-1} Pa.[S3] At the initial stage of pentacene film growth, separate islands of pentacene nucleate are formed from a common nucleation point (Figure S2).[S4] Then, as coverage is increased, the islands grow, coalesce with each other, and eventually link to form the first monolayer, in accompany with some second ML nuclei. When the thickness of pentacene is up to 2 ML, the first monolayer is almost completed, and the second ML have nucleated and grown up to form the dendritic islands. Meanwhile, the third and fourth islands form.[S5] With increasing the pentacene thickness increases to 5 ML, typical terrace-like islands are obtained, similar to the surface morphologies of 50 nm pentacene films (Figure 2b of the main text). These results suggest that the growth mode of pentacene films is not changed by the increase of P_{dep}.

SI 4. AFM images of pentacene films deposited under 2 and 10 Pa.

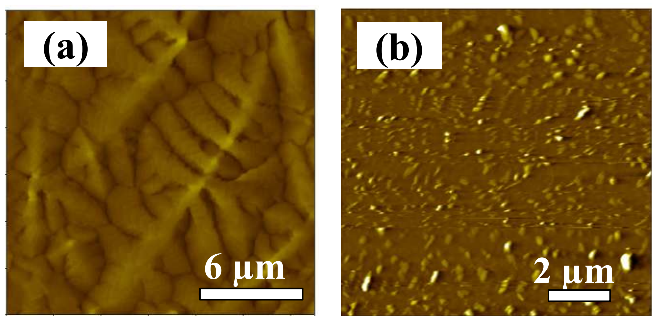

Figure S4. AFM images of pentacene films deposited under 2 (a) (18 µm × 18 µm) and 10 Pa (b) (10 µm × 10 µm).

SI 5. Distributions of *D* values of $F_{16}CuPc$, pentacene, TIPS-pentacene, and C_{60} molecules under different deposition pressures (P_{dep}).

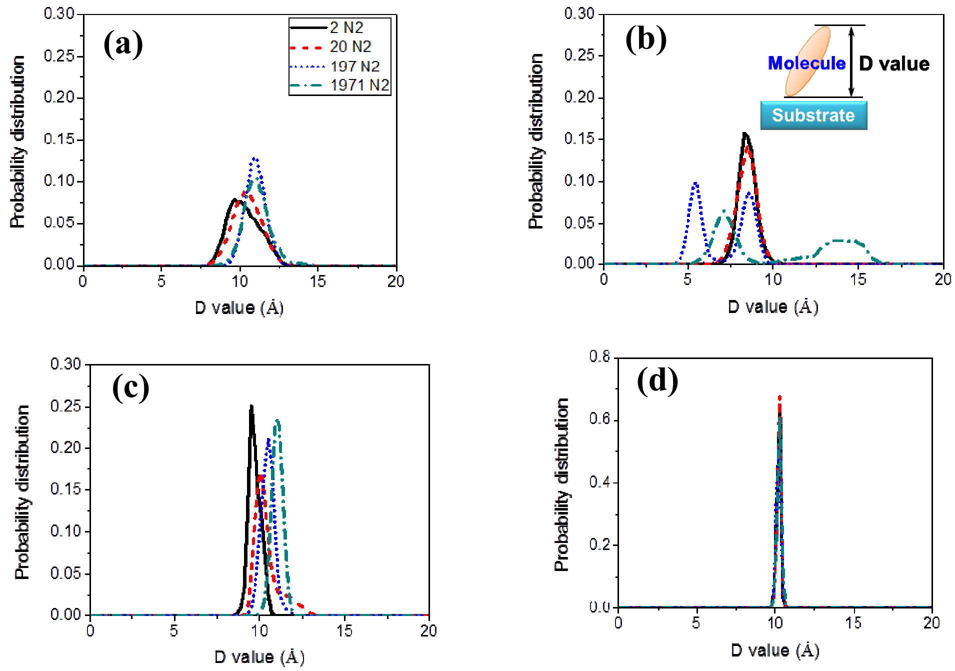

Figure S5. Distributions of *D* values of $F_{16}CuPc$ (a), pentacene (b), TIPS-pentacene (c), and C_{60} (d) molecules under different P_{dep}.

Note: The theoretical *D* value is defined as the sum of vertical height of molecule and van der Waals (vdW) radii of both the highest and lowest atoms in the molecule along the vertical direction. For $F_{16}CuPc$, pentacene, and TIPS-pentacene molecules, the theoretical *D* values are comparable with the experimental ones. For C_{60} molecules, the theoretical *D* value (ca. the diameter of a C_{60} molecule) is somewhat different from the experimental one (see inset of Figure 3h of the main text) (ca. twice the diameter of C_{60} in the face-centered cubic crystal), which doesn't influence the variation of *D* values with P_{dep}.

SI 6. XRD patterns of pentacene, TIPS-pentacene and C_{60} films deposited under different P_{dep}.

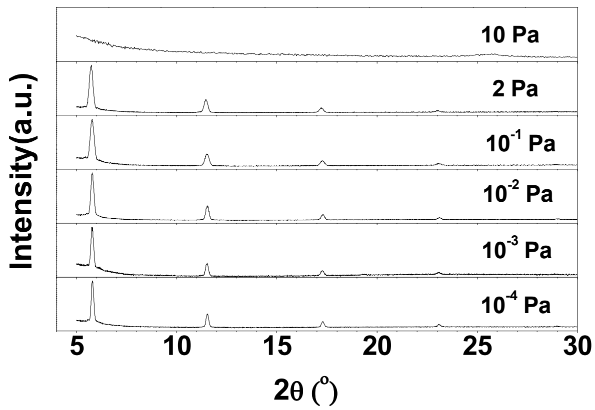

Figure S6. XRD patterns of pentacene films deposited under different P_{dep}.

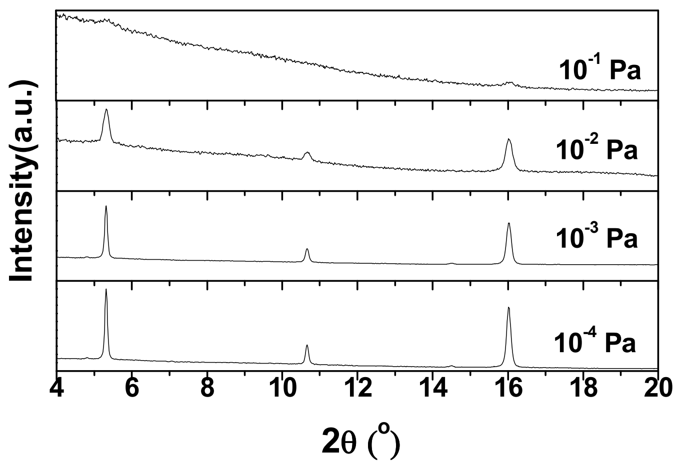

Figure S7. XRD patterns of TIPS-pentacene films deposited under different P_{dep}.

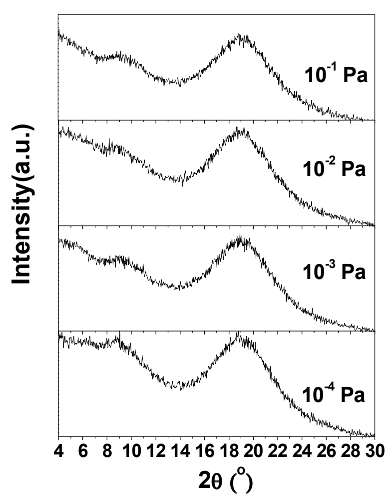

Figure S8. XRD patterns of C_{60} films deposited under different P_{dep}.

SI 7. Output characteristics of $F_{16}CuPc$, pentacene, TIPS-pentacene and C_{60} TFTs prepared under different P_{dep}.

$F_{16}CuPc$

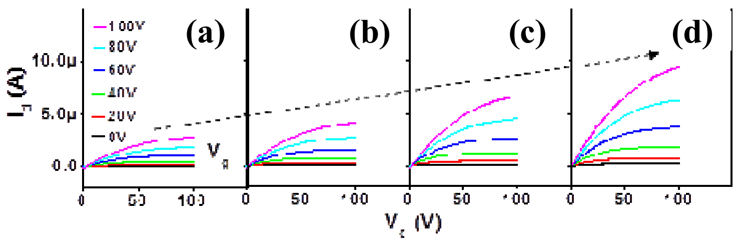

pentacene

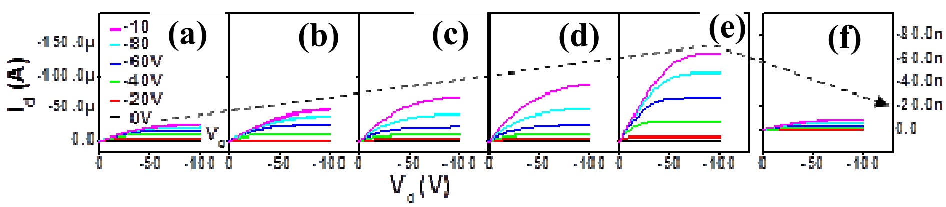

TIPS-pentacene

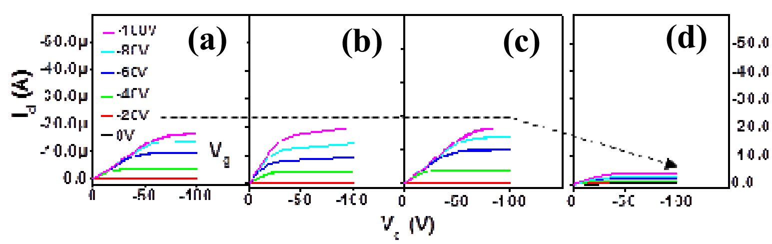

C_{60}

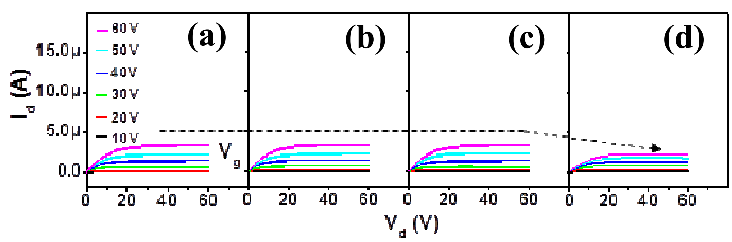

Figure S9. Output (I_d-V_d) characteristics of $F_{16}CuPc$, pentacene, TIPS-pentacene and C_{60} TFTs prepared under different P_{dep}. (a) 10^{-4} Pa, (b) 10^{-3} Pa, (c) 10^{-2} Pa, (d) 10^{-1} Pa, (e) 2 Pa, (f) 10 Pa. The dashed line and arrow schematically marks the changing tendency of I_d with P_{dep} for the same V_d and V_g. The different changing tendencies of I_d with P_{dep} for the $F_{16}CuPc$, pentacene, TIPS-pentacene and C_{60} TFTs result from the different evolutions of the morphologies and molecular packing structures for the corresponding organic films, similar to the change of carrier mobilities with P_{dep} in Figure 6 of the main text.

SI 8. Density functional theory calculations on carrier mobilities for model systems.

In order to further reveal the influence of packing structures on charge-transfer properties, we theoretically calculate the electron and hole mobilities of $F_{16}CuPc$ and pentacene dimers with a fixed the intermolecular distance (*r*) of 3.82 Å and 6.06 Å, respectively, as a function of *D* value. The charge hopping rates for $F_{16}CuPc$ and pentacene dimers are estimated according to the Marcus theory,[S6- S8]

$$k_{\text{h/e}} = \left(\frac{\pi}{\lambda_{\text{h/e}} k_B T}\right)^{1/2} \frac{t_{\text{h/e}}^2}{\hbar} \exp\left(-\frac{\lambda_{\text{h/e}}}{4k_B T}\right) \qquad \text{(S1)}$$

where k_B and $\hbar$ are the Boltzmann and Planck constants, respectively, and T is the temperature. For the charge hopping rates, there are two key parameters, the hole/electron reorganization energy, $\lambda_{h/e}$, and the hole/electron transfer integral, $t_{h/e}$ The hole/electron reorganization energy is calculated based on a simple model in the previous work.[S9, S10] The hole/electron transfer integral is directly evaluated from the Fock-matrix-based method,[S11, S12]

$$t_{\text{h/e}} = \left\langle \psi_{\text{HOMO/LUMO}}^{\text{Site i}} \,|\, \hat{F} \,|\, \psi_{\text{HOMO/LUMO}}^{\text{Site j}} \right\rangle \qquad \text{(S2)}$$

where $\psi_{\text{HOMO/LUMO}}^{\text{Site i}}$ and $\psi_{\text{HOMO/LUMO}}^{\text{Site j}}$ are the highest occupied molecular orbitals (HOMOs) and lowest unoccupied molecular orbitals (LUMOs) of two optimized monomers at the adjacent site *i* and *j*, respectively, and $\hat{F}$ is the Kohn-Sham Fock operator. Without consideration of the charge hopping probability, the hole/electron mobility, $\mu_{\text{h/e}}$, can be derived from the Einstein equation,[S13, S14]

$$\mu_{\text{h/e}} = \frac{e}{k_B T} D_{\text{h/e}} \approx \frac{e}{k_B T} \cdot \frac{1}{6} r^2 k_{\text{h/e}} \qquad \text{(S3)}$$

where *D* is the diffusion coefficient. The calculation results are shown in Figure S10.

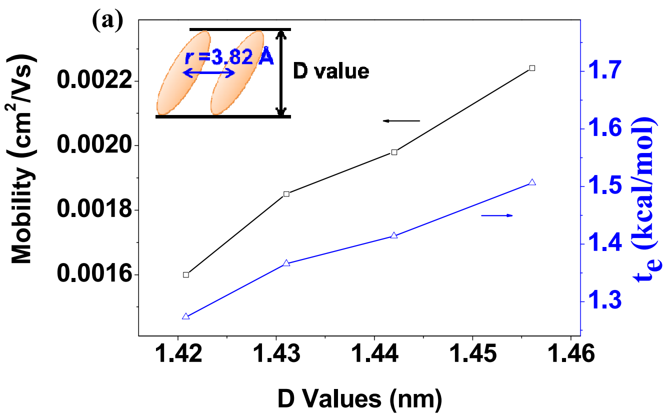

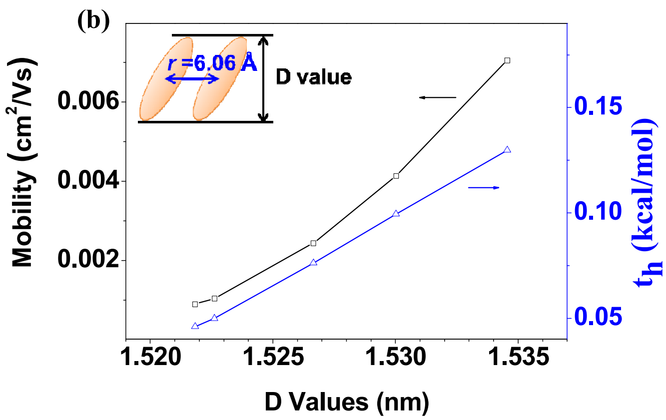

Figure S10. Carrier (electron/hole) mobilities and charge transfer integrals (t_e/t_h) of F_{16}CuPc (a) and pentacene (b) dimeric systems as a function of *D* value.

SI 9. AFM images and mobilities of C_{60} films with substrate temperatures of 150 and 180 ℃.

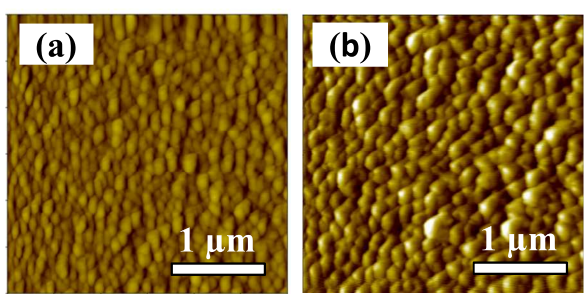

Figure S11. AFM images (3 μm × 3 μm) of C_{60} films with substrate temperature of 150 (a) and 180 ℃ (b).

Note: 40 nm C_{60} films were deposited under 150 and 180 ℃ with depsition rate of

0.01 nm/s and P_{dep} of and 10^{-4} Pa. Comparing their properties with those of C_{60} films with substrate temperature of 120 ℃ and P_{dep} of 10^{-4} Pa (Figure 6d of the main text.), the grain sizes increases from ca. 102 to 180 and 250 nm, while the mobilities decreases from ca. 0.20 to 0.07 and 0.02 cm^2/Vs, respectively. This result demonstrates that the grain size is not crucial to high mobility in C_{60} TFTs.

SI 10. Summary of the electrical parameters for $F_{16}CuPc$, pentacene, TIPS-pentacene, and C_{60} TFTs prepared under different P_{dep}. The average values of performance for each samples was obtained from eight devices.

Table S2

samples	P_{dep} (Pa)	Mobility (cm^2/Vs)	V_T (V)	I_{on}/I_{off}	S (V/dec)
$F_{16}CuPc$	10^{-4}	0.009±0.001	2.5±0.6	10^4–10^5	7.3±0.3
	10^{-3}	0.013±0.002	5.1±0.8	10^4–10^5	10.1±0.2
	10^{-2}	0.021±0.002	9.1±1.0	10^4–10^5	11.5±0.2
	10^{-1}	0.027±0.003	1.4±0.4	10^4–10^5	7.8±0.3
pentacene	10^{-4}	0.154±0.032	-18.9±1.1	10^5–10^7	1.1±0.2
	10^{-3}	0.238±0.041	-19.4±1.4	10^5–10^7	1.2±0.1
	10^{-2}	0.389±0.033	-29.6±2.0	10^5–10^6	4.0±0.5
	10^{-1}	0.562±0.050	-22.3±0.9	10^5–10^7	1.3±0.3
	2	0.703±0.071	-22.7±1.3	10^5–10^7	1.1±0.2
	10	$(2.56±1.00)\times10^{-4}$	-29.1±2.2	10^2–10^3	7.3±0.6
TIPS-pentacene	10^{-4}	0.234±0.030	-9.0±0.6	10^5–10^7	1.0±0.2
	10^{-3}	0.240±0.025	-20.5±1.2	10^5–10^7	1.4±0.1
	10^{-2}	0.230±0.027	-22.1±1.1	10^5–10^6	1.6±0.1
	10^{-1}	$(3.60±0.30)\times10^{-5}$	-52.8±2.3	10^2–10^3	2.2±0.4
C_{60}	10^{-4}	0.199±0.020	11.9±0.8	10^5–10^7	4.3±0.4
	10^{-3}	0.204±0.015	7.2±1.0	10^5–10^7	3.4±0.3
	10^{-2}	0.195±0.017	8.7±0.7	10^5–10^7	4.7±0.2
	10^{-1}	0.090±0.013	13.2±1.2	10^5–10^7	5.1±0.2

V_T: threshold voltage. I_{on}/I_{off}: on/off current ratio. S: sub-threshold slope.

Note: A high V_T is observed for the pentacene TFTs with P_{dep} of 10^{-2} Pa, indicating the high charge trap density at the pentacene/dielectric interface. The maximum interfacial trap density (N_{trap}) can be estimated from the following equation:[S15]

$$N_{trap} \approx \frac{C_i}{q}\left[\frac{qS\log(e)}{k_B T} - 1\right]$$

where C_i is the capacitance density of the gate dielectric, q is the electronic charge, S is the sub-threshold slope, k_B is Boltzmann's constant, and T is temperature. We estimate N_{trap} in pentacene TFTs with P_{dep} of 10^{-2} Pa to be 5.1×10^{12} cm^{-2}, while those in devices with P_{dep} of 10^{-4}, 10^{-3}, 10^{-1} and 2 to be 1.4×10^{12} cm^{-2}, 1.5×10^{12} cm^{-2}, 1.6×10^{12} cm^{-2} and 1.4×10^{12} cm^{-2}, respectively. A higher N_{trap} at the pentacene/dielectric interface in pentacene TFTs with P_{dep} of 10^{-2} Pa leads to the shift of V_T.

It has been demonstrated that the charge trap sites of pentcene TFTs mainly stem from the inter-grain boundaries between pentacene islands and the intra-grain boundaries in pentacene islands.[S16, S17] In grain boundaries, there should be many weak crystalline pentacene grains, which are the charge trap sites.[S17] From the XRD patterns, pentacene films with P_{dep} of 10^{-2} Pa show broadened (00l) peaks comparing to those of the pentacene films with P_{dep} of 10^{-4} and 10^{-3} Pa (Figure S6), indicating the decreased crystallite sizes. The crystallite size is an average measurement for pentacene films, including the islands with high crystallinity and small grains with weak crystallinity in grain boundaries (Figure S12a).[S18] Considering the slightly increased grain sizes and the decreased intergrain boundaries from AFM measurement (Figure 2b of the main text), the decreased crystallite sizes of the films with P_{dep} of 10^{-2} Pa means the increased small grains in intra-grain boundaries (Figure S12b). So the overall charge trap sites may be increased, leading to increased V_T. For the samples with P_{dep} of 10^{-1} and 2 Pa, although the high density of charge trap sites in intra-grain boundaries, that in inter-grain boundaries is very low due to the large islands (Figure S12c), resulting in the relatively low V_T of about -20 V compared that of pentacene films with P_{dep} of 10^{-2} Pa.

It is noticed that the traps in intra-grain boundaries may be not the deep traps, which have little effects on the mobility due to quenched by carriers.[S15, S19]

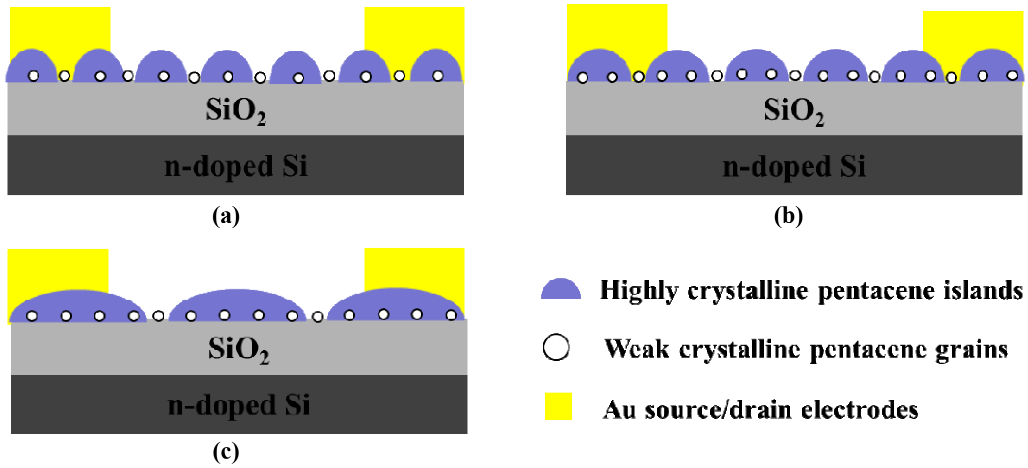

Figure S12. Schematic cross sections of pentacene TFTs with P_{dep} of 10^{-4} (a), 10^{-2} (b), and 10^{-1} Pa (c). The weak crystalline pentacene grains in iner- and intra-grain boundaries are generally the charge trap sites.

References

S1. Yokoyama, T.; Park, C. Bum.; Nagashio, K.; Kita, K.; Toriumi, A. Grain Size Increase in Pentacene Thin Films Prepared in Low-Pressure Gas Ambient. *Thin Solid Films* **2009**, *518*, 507– 509.

S2. Shtein, M.; Mapel, J.; Benziger, J. B.; Forrest, S. R. Effects of Film Morphology and Gate dielectric Surface Preparation on the Electrical Characteristics of Organic-Vapor-Phase-Deposited Pentacene Thin-Film Transistors. *Appl. Phys. Lett.* **2002**, *81*, 268–270.

S3. Ruiz, R.;. Choudhary, D.; Nickel, B.; Toccoli, T.; Chang, K.-C.; Mayer, A. C.; Clancy, P.; Blakely, J. M.; Headrick, R. L.; Iannotta, S.; et al. Pentacene Thin Film Growth. *Chem. Mater.* **2004**, *16*, 4497–4508.

S4. Meyer zu Heringdorf, F. J.; Reuter, M. C.; Tromp, R. M. Growth Dynamics of Pentacene Thin Fims. *Nature* **2001**, *412*, 517–520.

S5. Park, B.-N.; Seo, S.; Evans, P. G. Channel Formation in Single-Monolayer

Pentacene Thin Film Transistors. *J. Phys. D: Appl. Phys.* **2007**, *40*, 3506–3511.

S6. Marcus, R. A. Electron Transfer Reactions in Chemistry. Theory and Experient. *Rev. Mod. Phys.* **1993**, *65*, 599–610.

S7. Marcus, R. A. Chemical and Electrochemical Electron-Transfer Theory. *Annu. Rev. Phys. Chem.* **1964**, *15*, 155–196.

S8. Marcus, R. A. On the Theory of Oxidation-Reduction Reactions Involving Electron Transfer. *J. Chem. Phys.* **1956**, *24*, 966.

S9. Hutchison, G. R.; Ratner, M. A.; Marks, T. J. Hopping Transport in Conductive Heterocyclic Oligomers: Reorganization Energies and Substituent Effects. *J. Am. Chem. So*c. **2005**, *127*, 2339–2350.

S10. Brédas, J. L.; Beljonne, D.; Coropceanu, V.; Cornil, J. Charge-Transfer and Energy-Transfer Processes in π-Conjugated Oligomers lymers: A Molecular Picture. *Chem. Rev.* **2004**, *104*, 4971–5004; and references therein.

S11. Troisi, A.; Orlandi, G. The Hole Transfer in DNA: Calculation of Electron Coupling between Close Bases. *Chem. Phys. Lett.* **2001**, *344*, 509–518.

S12. Yang, X.; Li, Q.; Shuai, Z. Theoretical Modelling of Carrier Transports in Molecular Semiconductors: Molecular Design of Triphenylamine Dimer Systems. *Nanotechnology* **2007**, *18*, 424029.

S13. Deng, W.-Q.; Goddard, W. A. Predictions of Hole Mobilities in Oligoacene Organic Semiconductors from Quantum Mechanical Calculations. *J. Phys. Chem. B* **2004**, *108*, 8614.

S14. Yang, X.; Wang, L.; Wang, C.; Long, W.; Shuai, Z. Influences of Crystal Structures and Molecular Sizes on the Charge Mobility of Organic Semiconductors: Oligothiophenes. *Chem. Mater.* **2008**, *20*, 3205–3211.

S15. McDowell, M.; Hill, I. G.; McDermott, J. E.; Nernasek, S. L.; Schwartz, J. Improved Organic Thin-Film Transistor Performance Using Novel Self-Assembled Monolayers. *Appl. Phys. Lett.* **2006**, *88*, 073505.

S16. Yang, H.; Shin, T. J.; Ling, M.-M.; Cho, K.; Ryu, C. Y.; Bao, Z. Conducting AFM and 2D GIXD Studies on Pentacene Thin Films. *J. Am. Chem. Soc.* **2005**, *127*, 11542–11543

S17. Tello, M.; Chiesa, M.; Duffy, C. M.; Sirringhaus, H. Charge Trapping in Intergrain Regions of Pentacene Thin FilmTransistors. *Adv. Funct. Mater.* **2008**, *18*, 3907–3211.

S18. Chou, W. Y.; Mai, Y. S.; Cheng, H. L.; Yeh, C. Y.; Kuo, C. W.; Tang, F. C.; Shu, D. Y.; Yew, T. R.; Wen, T. C. Correlation of Growth of Pentacene Films at Various Gas Ambience Conditions to Organic Field-Effect Transistor Characteristics. *Org. Electron.* **2006,** *7*, 445–451.

S19. Yin, S.; Yang, Y.; Lv Y. Theoretical Study the Trap and Carrier-Density Ddependent Electron Mobility in Pentacene AB-Plane By the Steady Master Eequation. *Synth. Met.* **2010**, *160*, 1241–1246.